ACS Biomaterials SCIENCE & ENGINEERING

Article

pubs.acs.org/journal/abseba

Low Cytotoxicity and Genotoxicity of Two-Dimensional MoS_2 and WS_2

Jennie H. Appel,[†] Duo O. Li,[‡] Joshua D. Podlevsky,[§] Abhishek Debnath,[§,∥] Alexander A. Green,[§,∥] Qing Hua Wang,[‡] and Junseok Chae*[,†]

[†]School of Electrical, Computer, and Energy Engineering, [‡]Materials Science and Engineering, School for Engineering of Matter, Transport and Energy, [§]School of Molecular Sciences, and [∥]Center for Molecular Design and Biomimetics, The Biodesign Institute, Arizona State University, Tempe, Arizona 85287, United States

Supporting Information

ABSTRACT: Atomically thin transition-metal dichalcogenides (TMDs) have attracted considerable interest because of their unique combination of properties, including photoluminescence, high lubricity, flexibility, and catalytic activity. These unique properties suggest future uses for TMDs in medical applications such as orthodontics, endoscopy, and optogenetics. However, few studies thus far have investigated the biocompatibility of mechanically exfoliated and chemical vapor deposition (CVD)-grown pristine two-dimensional TMDs. Here, we evaluate pristine molybdenum disulfide (MoS_2) and tungsten disulfide (WS_2) in a series of biocompatibility tests, including live−dead cell assays, reactive oxygen species (ROS) generation assays, and direct assessment of cellular morphology of TMD-exposed human epithelial kidney cells (HEK293f). Genotoxicity and genetic mutagenesis were also evaluated for these materials via the Ames Fluctuation test with the bacterial strain *S. typhimurium* TA100. Scanning electron microscopy of cultured HEK293f cells in direct contact with MoS_2 and WS_2 showed no impact on cell morphology. HEK293f cell viability, evaluated by both live−dead fluorescence labeling to detect acute toxicity and ROS to monitor for apoptosis, was unaffected by these materials. Exposure of bacterial cells to these TMDs failed to generate genetic mutation. Together, these findings demonstrate that neither mechanically exfoliated nor CVD-grown TMDs are deleterious to cellular viability or induce genetic defects. Thus, these TMDs appear biocompatible for future application in medical devices.

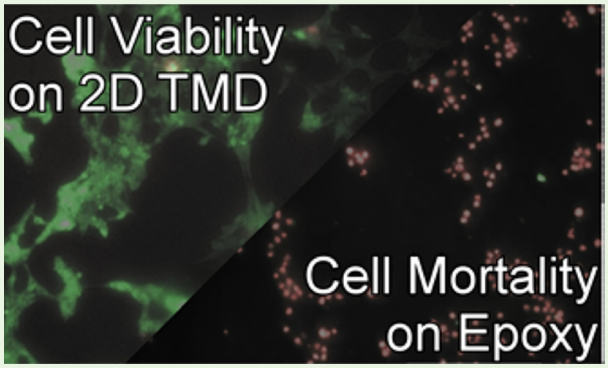

KEYWORDS: *biocompatibility, tungsten disulfide, molybdenum disulfide, oxidative stress, bacterial mutagenesis, two-dimensional materials, transition-metal dichalcogenides*

INTRODUCTION

Transition metal dichalcogenides (TMDs) are a class of layered materials with the general formula MX_2, where M represents a transition metal (Mo, W, Ta, Nb, etc.) and X represents a chalcogen (S, Se, Te). In the past few years, studies of atomically thin 2D TMDs have expanded rapidly due to their impressive electrical, optical, and structural properties.[1] Semiconducting TMDs like MoS_2 and WS_2, have band gaps that transition from indirect to direct when their thicknesses are reduced from bulk to monolayer.[2] Monolayer TMDs have been integrated into field-effect transistors which possess both high on/off current ratios and reasonable carrier mobilities,[3] good photoluminescence at room temperature,[4] and high elastic strength.[5] In the biomedical fields, fullerene-like TMD nanoparticles have been used for their tribological properties to reduce friction in numerous applications.[6] Solid lubricants containing fullerene-like WS_2 were commercialized in 2008.[7] In orthodontia, WS_2 nanoparticles have been embedded in the stainless steel wires used to manipulate teeth, and Redlich et al. reported that incorporation of WS_2 reduced overall frictional force in this application by 54%.[8] Additional tribological applications include gels impregnated with WS_2 or MoS_2 nanoparticles to reduce friction in endoscopic procedures[9] and bone tissue engineering.[10]

Despite existing biomedical applications using TMDs and the still-emerging applications of 2D TMDs, few investigations into the biocompatibility and toxicity of TMDs have been performed. So far, initial in vivo toxicology tests of fullerene-like WS_2 nanoparticles on mammals found no toxic effects.[8] Cytotoxicity examinations of fullerene-like MoS_2 and WS_2 on human cell-lines, salivary gland cells[11] and A549,[12] found that they are nontoxic to cells as cell viability remained high after prolonged exposure to TMDs.[11,12] Recently, Teo et al. reported the varying cytotoxicity of lithiated forms of WS_2, MoS_2 and WSe_2, which are chemically and electronically different from their pristine forms. In that study, human lung carcinoma

Received: November 5, 2015
Accepted: February 22, 2016
Published: February 22, 2016

DOI: 10.1021/acsbiomaterials.5b00467
ACS Biomater. Sci. Eng. 2016, 2, 361−367

epithelial cells (A549) were used to show that lithiated WS_2 and MoS_2 are extremely biocompatible while lithiated WSe_2 caused dose-dependent toxicological effects.[13] Although lithiated TMDs are being explored as vectors for drug delivery and photothermal therapy,[14] these chemically treated TMDs possess metallic conductivity and thus lack the highly desirable photoluminescent properties of pristine TMDs. These fundamental differences in the electronic and optical properties of lithiated and pristine TMDs suggest that these phases may also interact with biological systems in very different ways. Moreover, future medical application of TMDs in areas like optogenetics will require pristine materials that retain their fluorescence. Consequently, there is an urgent need for systematic and in-depth biocompatibility and toxicity studies on pristine, unfunctionalized TMDs.

Here we report a detailed study examining the biocompatibility of pristine two-dimensional WS_2 and MoS_2 toward human epithelial kidney cells, HEK293f. Studying the impact of fine particulates on HEK293f is particularly relevant because particulates of this kind have a tendency to accumulate in the kidneys.[15] We examine the effects of culturing HEK293f cells directly in contact with large flakes, or sheets, of thin TMDs using a fluorescent calcein-AM/ethidium homodimer-1 live-dead assay and a fluorogenic probe designed to measure reactive oxygen species (ROS) in live cells. We also examined the potential bacterial mutagenicity of these 2D nanoparticulates by performing an Ames Fluctuation assay using *S. typhimurium* TA100. Our comprehensive set of experiments show that 2D and particulate forms of TMDs exhibit very low cytotoxicity and genotoxicity effects, and are thus attractive materials for future biomedical applications.

MATERIALS AND METHODS

TMD Synthesis: Flakes and Sheets. Crystalline flakes of TMDs were exfoliated from bulk crystals of WS_2 (2D Semiconductors) and MoS_2 (SPI Supplies) using the scotch tape method onto substrates (oxygen plasma treated PDMS). Large area sheets of MoS_2 were synthesized using chemical vapor deposition onto SiO_2/Si substrates that were cleaned by sonication in acetone for 5 min, in isopropanol for 5 min, and oxygen plasma for 10 min. The precursors were 15 mg molybdenum trioxide, MoO_3 (≥99.5%, Sigma-Aldrich) and 100 mg sulfur, S (99.5%, Alfa Aesar). Growth occurred in a 1 in. diameter tube furnace (Lindberg). The MoO_3 precursor was placed in the center of the heating zone in a quartz boat with the SiO_2/Si substrate placed above it, face down. The S was placed at the edge of the heating zone. The CVD growth occurred at vacuum pressure (1.37 Torr) with 300 sccm Ar gas flow. The furnace was first heated to 650 °C at a rate of 16 °C/min, held at 650 °C for 30 min, and rapidly cooled to room temperature. The mechanically exfoliated and CVD-grown samples were used for the live−dead assay and the SEM assay.

TMD Synthesis: Particulates. TMD particulates were prepared from bulk WS_2, bulk MoS_2, and CVD-grown MoS_2 by bath sonication. Fragments of bulk MoS_2 and WS_2 were weighted, placed in sterile water or tissue culture media and submerged in an ultrasonic bath until only the ultrafine particulates remain. CVD particulates were prepared by sonicating the MoS_2-covered SiO_2/Si substrates until all traces of MoS_2 were removed from substrates. The concentrated particulate suspensions were then diluted to obtain the various concentrations used in the assays.

TMD Characterization: Raman Spectroscopy, Scanning Electron Microscopy, Surface Charge, and Fluorescence. Mechanically exfoliated WS_2, mechanically exfoliated MoS_2, and CVD-grown MoS_2 were all deposited on Si wafers with a 300 nm SiO_2 capping layer. Raman spectroscopy was conducted using a WITec Alpha300R Confocal Raman Imaging System with 532 nm excitation, 300 μW laser power and a 100X objective lens.

TMD particulates were analyzed using SEM. A small amount of the liquid containing each type of fragment was placed onto a glass slide and left until completely evaporated. Then the glass slide was sputter coated with a layer of gold, approximately 10 nm thick, and imaged with a scanning electron microscope (Hitachi S-4700-II).

TMD particulates were evaluated for surface charges using a Zetasizer Nano ZS to evaluate zeta potential with a mechanically exfoliated MoS2 particulate sample at a concentration of 1 mg/mL. TMD particulates were also evaluated for fluorescence (Horiba Nanolog) using a range of excitation wavelengths (400−600 nm) and emission wavelengths (600−800 nm). These measurements did not reveal any photoluminescence peaks attributable to MoS_2.

Cell Culture. HEK293f cells (Invitrogen) were grown in Eagle's minimum essential medium (EMEM) (ATCC). Media was supplemented with 10% fetal bovine serum (FBS, Life Technologies), and 1X penicillin/streptomycin (Sigma-Aldrich). Cells were maintained in a 5% CO_2 environment at 37 °C. Cells at 80% confluency were trypsinized (Invitrogen) for 1 min at 37 °C and washed with media supplemented with 10% FBS. Approximately 1×10^5 cells were applied to each material and incubated in culture media with at 5% CO_2 at 37 °C.

Live−Dead Assay. Mechanically exfoliated tungsten disulfide, mechanically exfoliated molybdenum disulfide, CVD-grown molybdenum disulfide, silver, epoxy, graphite, and plain PDMS were prepared for the live/dead assay and all were placed on oxygen plasma cleaned PDMS substrates. Gold and silver were sputter coated onto the PDMS substrate and epoxy was mixed then spread onto the PDMS. HEK293f cells were cultured on 24 subsections of each material and incubated at 37 °C in a 5% CO_2 environment for 4, 12, 24, and 48 h. After the desired time interval, samples were placed in a solution containing 2 μM calcein AM and 4 μM ethidium homodimer-1 (Life Technologies, viability/cytotoxicity kit for mammalian cells) and incubated at room temperature for 30 min, without exposure to light, then imaged under a fluorescent confocal microscope (Nikon Eclipse TE2000-U).

For the live−dead assay a minimum of 10 technical replicates of each material were examined at every time interval. The numbers of live and dead cells in direct contact with the material was tallied, and then the average percent of live cells was quantified from all samples. The standard error was also quantified for each time and material.

Cell Morphology Scanning Electron Microscopy Preparation and Imaging. Large flakes and sheets of each TMD was used for SEM imaging, all control materials from the live−dead assay were also imaged. HEK293f cells were cultured in direct contact with the all materials for 24 h. Then cells were washed 3 times in PBS, fixed in 4% paraformaldehyde in 1X PBS for 10 min at 37 °C, and washed twice with 1X PBS. Samples were then dehydrated serially, 10 min transfers through 50, 60, 70, 80, 90, and 100% ethanol. Then devices were sputter coated with a layer of gold, approximately 10 nm thick, and imaged using a scanning electron microscope (Hitachi S-4700-II).

Reactive Oxygen Species (ROS) Assay. TMD particulates and copper particulates were used for the ROS assay. Solid copper (8.33 mg) was placed in 1 mL of EMEM supplemented with 10% FBS, then placed in an ultrasonic bath for 7 min to degrade the copper into particles. HEK293f cells were cultured to 80% confluency then exposed to various concentrations of each TMD particulate (100, 10, 1, 0.1 μg/mL) and copper (8.33 mg/mL) for 1, 8, and 24 h. After each time interval the proprietary ROS fluorogenic probe (Molecular Probes, CellROX) was added to a concentration of 5 μg/mL to the culture well and incubated for 30 min at 37 °C, then the culture well was washed 3 times with 1X PBS to remove any unbound ROS fluorogenic probe and visualized under a fluorescent confocal microscope (Nikon Eclipse TE2000-U) using 485/520 (nm) excitation/emission.

For the ROS assay, a minimum of eight technical replicates of each TMD concentration, the positive copper control and the untreated negative control were examined at each exposure time. Fluorescence intensity was measured using ImageJ software, and then intensity was averaged over the full area of the image. Standard error was calculated by determining the standard deviation between each technical replicate and dividing by the square root of the number of technical replicates.

DOI: 10.1021/acsbiomaterials.5b00467
ACS Biomater. Sci. Eng. 2016, 2, 361−367

Significance was calculated by determining the chi-squared value, in comparison to the copper-positive control, and then using a standard chi-squared distribution table to determine *p*-value.

Ames Fluctuation Test of Reverse Mutation. TMD particulates were used for the Ames Fluctuation test of reverse mutation. Particulates were sterilized using heat and 70% ethanol. The Ames Fluctuation assay (Environmental Bio-Detection Products Inc.) was performed according to the manufacturer's instructions. Briefly, the reaction mixture containing Davis-Mingioli salts, D-glucose, bromocresol purple, D-Biotin and L-histidine was mixed with the particulates and purified water to concentrations of 100, 10, 1, and 0.1 μg/mL. TA100 bacteria, grown overnight to turbidity, was added to each concentration of TMD particulates. Each mixture was then distributed into 20 wells of a 96 well plate, along with the positive control: mutation generating sodium azide and negative control: untreated bacteria. All plates were placed in a sealed bag, to prevent evaporation, and incubated at 37 °C for 3–6 days. Results were read by visual inspection of each well, with yellow or turbid wells considered positive for bacterial mutation and purple wells considered negative for mutation.

For the Ames Fluctuation reverse mutation assay, 20 wells of each sample and the controls were prepared. The number of yellow and purple wells, meaning positive and negative for mutation, respectively, were tallied and the percentage of revertants was calculated. Significance was calculated by determining the chi squared value, in comparison to the sodium azide-positive control, and then using a standard chi squared distribution table to determine the *p*-value.

RESULTS

Synthesis and Characterization of WS_2 and MoS_2. Thin flakes of WS_2 and MoS_2 were prepared from bulk crystalline samples by mechanical exfoliation using adhesive tape. We examined mechanically exfoliated WS_2 (ME-WS_2) and MoS_2 (ME-MoS_2) flakes that were around 8–10 μm in diameter (Figure 1a, b). Large area, continuous, thin films of bilayer, trilayer and few-layer MoS_2 were also synthesized using CVD (CVD-MoS_2) (Figure 1c). Material size is of particular concern for cell viability because HEK293f cells are known to take up foreign materials via endocytosis.[16] However, it is unlikely that the flakes or sheets of WS_2 and MoS_2 will permeate a cell membrane because they are of similar size to that of the cell (typically 20 μm in diameter). Additionally materials larger than 100 nm in diameter typically do not undergo endocytosis by HEK293f cells.[16,17]

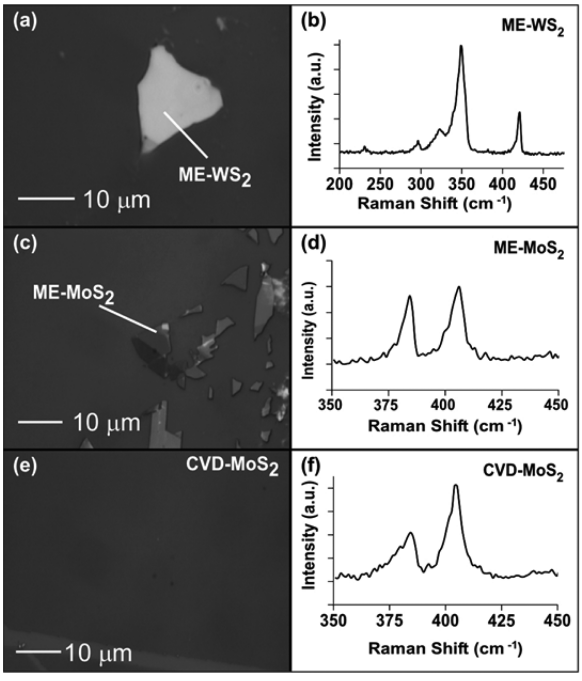

Figure 1. Scanning electron microscopy (SEM) images (a, c, e) and Raman spectra (b, d, f) of (a, b) mechanically exfoliated few-layer WS_2 (ME-WS_2), (c, d) few-layer ME-MoS_2, and (e, f) chemical vapor deposition grown (CVD)-MoS_2.

We characterized these TMD samples using Raman spectroscopy to estimate their thicknesses, as shown in Figure 1d–f. Characteristic peaks corresponding to the A_{1g} and E^1_{2g} phonons for MoS_2 and WS_2 are observed, and the difference between them is used to identify the layer numbers. For our ME-WS_2 flakes the observed peak difference of 70.2 cm^{-1} corresponds to 5 to 8 atomic layers;[18] for our ME-MoS_2 the difference of 21.9 cm^{-1} corresponds to 3 to 4 atomic layers;[19] for our CVD-MoS_2 the difference of 20.7 cm^{-1} corresponds to 2 to 3 atomic layers.[19] Material thickness is of particular concern for cell viability: if that material becomes "free floating" it may slice the cell membrane and induce death, as shown by Liao et al. for monolayer graphene and graphene oxide which slice red blood cells.[20] We avoid this issue by placing each material onto an inert substrate like polydimethylsiloxane (PDMS) or glass, where we can exclusively examine the interaction between the material surface and the cells.

Cellular Viability and Acute Toxicity Screening. To determine human cell viability following exposure to TMDs, we performed a fluorescence-based live–dead assay. HEK293f cells were exposed to ME-WS_2, ME-MoS_2, and CVD-MoS_2 for various time intervals. Then cells were fluorescently labeled as live using calcein-acetoxymethyl (calcein AM) or dead using ethidium homodimer-1. Calcein AM passively crosses the cell membrane where it is converted into green fluorescent calcein by intracellular esterases in live cells.[21] Ethidium homodimer-1 exclusively enters cells via damaged cell membranes and undergoes a 40-fold enhancement of fluorescence when bound to nucleic acids in the nucleus of dead or dying cells.[22] In Figure 2a–c, the green regions indicate living cells,

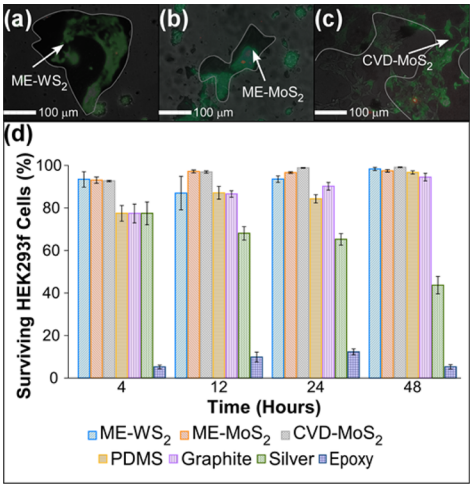

Figure 2. Cellular viability assay showing fluorescence images of HEK293f cells in direct contact with TMD flakes/sheets. (a–c) Green color shows live cells and red color show dead cells. The panels are for (a) ME-WS_2 (b) ME-MoS_2, and (c) CVD-MoS_2. (d) Overall cell viability of different control materials and different TMDs at as a function of time.

DOI: 10.1021/acsbiomaterials.5b00467
ACS Biomater. Sci. Eng. 2016, 2, 361–367

while the red spots indicate the nuclei of dead cells. These images clearly show that the majority of HEK293f cells exposed to ME-WS_2, ME-MoS_2, and CVD-MoS_2 after 24 h are alive (green) and only a few cells have died (red), indicating that these TMDs in the mechanically exfoliated and CVD-grown forms are not acutely toxic to HEK293f cells. Over time, the percentage of surviving HEK293f cells increases if those cells are in contact with ME-WS_2, ME-MoS_2, CVD MoS_2, PDMS, or graphite. In contrast, the percentage of surviving cells decreases when in contact with silver and remains low (~10%) when in contact with acutely toxic epoxy (Figure 2d). HEK293f cells undergo mitosis at a rate of approximately once every 23 to 24 h,[23] thus over a 48 h time period cells should double twice. Because of the doubling rate, cells in contact with a biocompatible material show an increase in percentage of survivability. This result indicates that MoS_2 and WS_2 in these thin, large-area forms are nontoxic.

Cellular Adhesion to Transition-Metal Dichalcogenides. We investigated the nature of the interaction between cells and each material by scanning electron microscopy (SEM) imaging of HEK293f cells cultured for 24 h in direct contact with either TMDs or epoxy as shown in Figure 3. The images

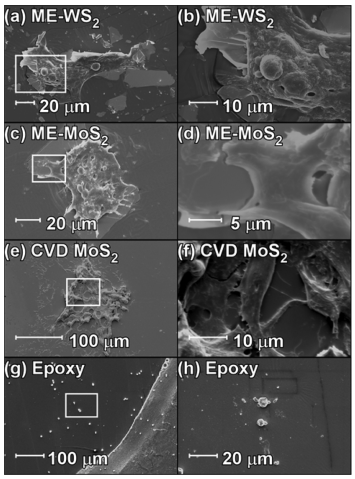

Figure 3. SEM images showing viable HEK293f cells adhered to (a, b) ME-WS_2, (c, d) ME-MoS_2, (e, f) CVD-MoS_2, and (g, h) epoxy. The regions indicated by rectangles in the left panels are shown magnified in the right panels.

on the left side (Figure 3a, c, e) provide an overview of cells interacting with large surface areas of each material. The images on the right side (Figure 3b, d, f) show a magnified view of HEK293f interaction with each material. In the case of ME-WS_2, ME-MoS_2, and CVD-MoS_2, filopodia spread upon the surface of each respective material indicating good cellular adhesion and healthy cell morphology. Additionally, cells interact directly with each respective material, as observed directly by the presence and arrangement of filopodia. In contrast, in Figure 3g, h cells up to 300 μm away from epoxy and in direct contact show the same rounded morphology, which indicates cellular toxicity. Observations based on control materials, PDMS, graphite, and silver are provided in Figure S1. These comparison materials were chosen because of their range of biocompatibilities, from the very biocompatible graphite[24] and PDMS[25] to cytotoxic silver[26] and acutely toxic epoxy. The observed interaction between HEK293f cells and TMDs indicates that not only are cells viable when exposed to TMDs but they thrive in contact with them.

Oxidative Stress Assays. In biomedical implants, particulates are generated as the body breaks down implanted materials,[27] which can then infiltrate cells and interfere with basic cellular function. This process occurs by exposing the implant to a harsh, low pH environment; encapsulating it in proteins and eventually fibrous tissue; and surrounding it with macrophage cells that combine to form foreign body giant cells.[27] To investigate the potential for TMD-based particulates to influence cellular activities in the body, we produced micro- to nanoscale TMD particulates and measured their influence on HEK293f cells. We produced TMD particulates by applying ultrasonic agitation to crystals of WS_2 and MoS_2, and CVD-grown MoS_2. Histograms of particulate dimensions and representative SEM images of the particulates are shown in Figure 4. These particulates have average diameters of about

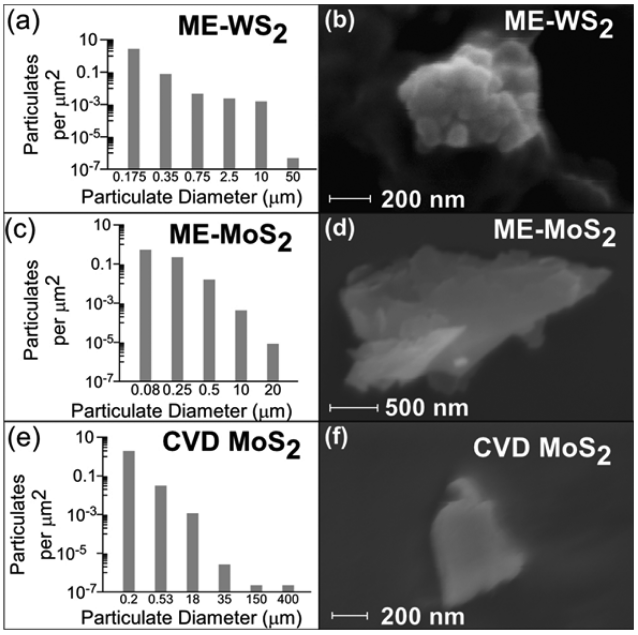

Figure 4. TMD particulates. (a, c, e) Histograms showing particulate diameters and (b, d, f) SEM images of representative particulates for (a, b) ME-WS_2, (c, d) ME-MoS_2, and (e, f) CVD-MoS_2.

200−300 nm. As endocytosis typically occurs in particles that are smaller than 100 nm,[16,17] the sizes of these particulates should prevent endocytosis. Additionally, we evaluated ME-MoS_2 particulates for surface charges using zeta potential. This allows us to evaluate cell viability risks due to surfaces charges. We found a surface charge of -22.87 ± 0.17 mV for ME-MoS_2. On the basis of a previous study by Ayala et al.,[28] a negative surface charge should not interfere with either internal or external cellular mechanisms. By varying the volume of the solution-phase TMDs we added to the cell growth media, we were able to examine cellular viability after exposure to various concentrations of particulate TMDs.

Materials that are not acutely toxic can still compromise cell viability by triggering oxidative stress, which commonly induces programmed cell death (apoptosis).[29] We exposed cells to particulates of TMDs and looked for an elevation in the amount of reactive oxygen species (ROS) using a proprietary cell-permeable fluorogenic probe (Figure S2). The fluorogenic probe is oxidized when interacting with ROS and then the

DOI: 10.1021/acsbiomaterials.5b00467
ACS Biomater. Sci. Eng. 2016, 2, 361−367

oxidized form of the reagent binds to DNA and fluoresces.[30] Therefore, the fluorescent intensity directly corresponds to the amount of ROS generated by the cells. We determined the fluorescence intensity as a measure of ROS level at various concentrations of particulate TMDs for multiple exposure times (Figure 5) as well as for the flake/sheet forms of TMDs after 12

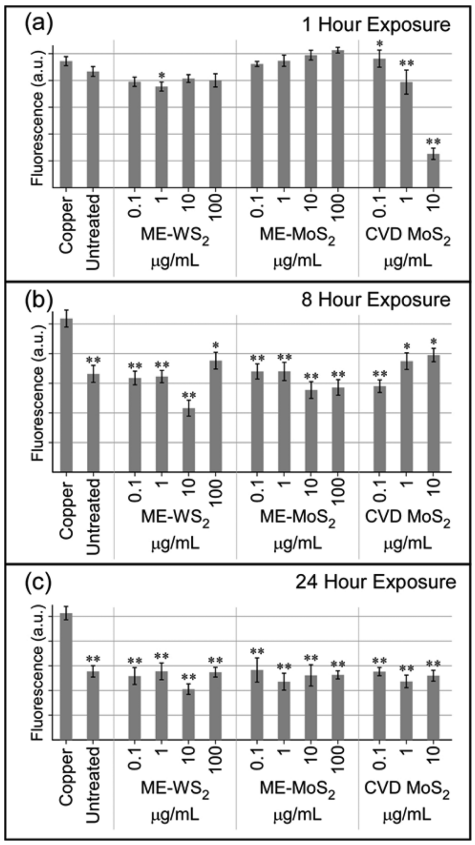

Figure 5. Fluorescence intensity plots measuring reactive oxygen species (ROS) generation for various TMD particulates and a copper positive control. TMD particulates do not generate significant levels of ROS after exposures of (a) 1, (b) 8, and (c) 24 h.

h of exposure (Figure S3). For comparison, we also used copper, a known generator of ROS, as a positive control.[31] A CVD MoS_2 concentration of 100 μg/mL was not tested due to the difficulty in fabricating sufficient amounts of MoS_2 via CVD to achieve that concentration. Additionally we attempted to track the TMD particulates via fluorescent microscopy, but we did not detect any photoluminescence signals even in the TMD particulate samples before cellular exposure. This is likely because we have primarily multilayer particulates that have an indirect bandgap and do not emit photoluminescence.[32] After 1 h of exposure to TMDs, there was no significant difference in fluorescence intensity between the untreated cells, the cells exposed to TMD particulates, and the cells exposed to copper (Figure 5a). However, after 8 h of exposure to TMD particulates, all concentrations and the untreated cells showed a significantly lower fluorescence intensity from the ROS-generating copper control (Figure 5b). Corresponding *p*-values in Figure 5 of these measurements are marked with * if they are less than 0.1 or ** if they are less than 0.05. After 12 h of exposure to TMD flakes/sheets and PDMS cells showed significantly lower fluorescence intensity from the ROS-generating copper control (Figure S3). After 24 h of exposure to TMD particulates at all concentrations and untreated cells show a significant difference in fluorescence intensity from the ROS-generating copper control (Figure 5c). Additionally we evaluated the viability of HEK293f cells, via live-dead assay, after 48 h exposure to particulates of ME-MoS_2, and found that 98% of cells remained viable during this time period (Figure S4). Measurements of ROS level show that particulates generated from ME-WS_2, ME-MoS_2, and CVD-MoS_2 do not induce ROS, even in concentrations as high as 100, 100, and 10 μg/mL, respectively. Hence, the solution phase TMD particulates do not activate this pathway to programmed cell death, even after 24 h exposure.

Mutagenicity Assays. We evaluated the effect of TMD particulates on mutagenicity using Ames Fluctuation assays. The Ames assay employs strains of *Salmonella typhimurium* with loss-of-function mutations in the genes for histidine synthesis. When these strains gain the ability to grow in histidine-free environments, they must do so by acquiring compensatory mutations that enable them to regain histidine synthesis capability. Consequently, when the bacteria are exposed to a mutagen, a greater fraction of them will acquire beneficial mutations and thrive without histidine. For this study, we used *S. typhimurium* tester strain TA100, which has a base-pair mutation, the most common type of genetic mutation. After 3 days of exposure to various concentrations of TMD particulates, the TA100 bacterial strain showed no significant mutation as shown in Figure 6. A significantly lower percentage of revertants was observed in untreated and TMD particulate treated samples. Significance was determined using p-values (** if they are less than 0.1 or * if they are less than 0.05) calculated referencing the positive highly mutagenic control, sodium azide. This mutation assay yields a color change triggered by the growth of bacteria, in a nonhistidine environment. Although, there was a low level of mutation that occurred for each TMD concentration, ranging from 5 to 25% of the total replicates. This was anticipated because random mutation easily occurs in this bacterial strain, as 10–15% of untreated negative control samples regained histidine synthesis, as shown in Figure S5. Thus, we can extrapolate that particulate TMDs are not a mutagenic agent for TA100, and therefore do not introduce base-pair substitutions.

DISCUSSION

The results of the wide variety of assays we have conducted all point to the excellent biocompatibility of 2D TMDs toward mammalian tissue cells and bacteria. First, our live–dead assays showed no acute toxicity. Cells touching or in close proximity to the 2D TMDs show excellent survival, as shown in Figure 2. In contrast to other cell viability tests that rely on the conversion of extracellular dehydrogenases,[33] which can be influenced by the presence of nanoparticles,[34] these fluorescence tests do not have that complication and are thus more suitable for evaluating nanostructured materials. In a previous study by Teo et al., lithiated forms of WS_2 and MoS_2 are evaluated for biocompatibility, but these lithiated forms are fundamentally different than pristine TMDs in that they are metallic rather than semiconducting, and chemically quite different.[13] In many potential biomedical applications for TMDs, we anticipate that the structural integrity, semiconducting electronic properties, and optical properties of pristine TMDs will be preferred over lithiated forms.

Our evaluation of cell morphology with SEM imaging of HEK293f cells showed that the cells have excellent adhesion

DOI: 10.1021/acsbiomaterials.5b00467
ACS Biomater. Sci. Eng. 2016, 2, 361–367

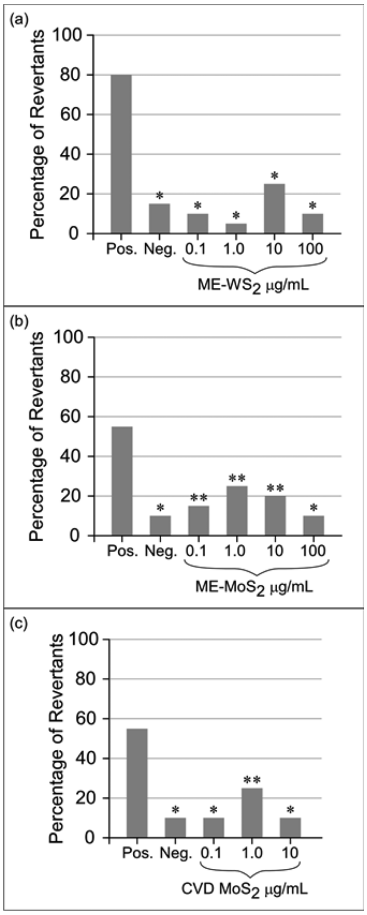

Figure 6. Mutagenicity measurement by Ames fluctuation test. The percentage of bacterial revertants after 3 days is calculated for positive controls of sodium azide, negative control of untreated bacteria, and varying concentrations of particulates of (a) ME-WS_2, (b) ME-MoS_2, and (c) CVD-MoS_2.

and interaction with the TMDs as indicated by the presence of multiple filopodia In contrast, known toxic materials yielded weak adhesion and rounded cells. The only other related study to our knowledge, Goldman et al., examined fullerene-like WS_2 nanoparticles,[11] rather than 2D forms as we show here, which have very different physical properties.

The ROS generation tests using nanoparticulates showed that TMDs have far lower levels of ROS compared to copper, a known ROS generator, for several exposure times, as shown in Figure 5. We observed time-dependent changes in fluorescence due to ROS that likely indicate the time necessary for HEK293f cells to undergo apoptosis, which ranges from 6 to 9 h.[35] A previous study by Kou et al. using lithiated nanosheets of MoS_2[36] also showed no significant generation of ROS.

Finally, because genetic modifications can lead to long-term health risks, we evaluated genotoxicity of TMD particulates using the Ames Fluctuation assay. If particulates are to induce genetic mutations, they are likely to do so by two mechanisms: (1) smaller particles can enter the cell and directly disrupt cellular activity, and (2) larger particles can block and disrupt the function of porins, which are important for the transfer of materials into the cell. Because we have a range of particle sizes in our dispersions, it is conceivable to have both modes of genotoxicity. However, our results showed no significant genotoxicity for any of our 2D TMD preparations, as shown in Figure 6. Thus, we believe that the smaller particles are likely not being taken up into the cells at a significant rate, and that the larger particles are ineffective at blocking porins.

CONCLUSION

We have performed an extensive study of the biocompatibility of different pristine forms of the TMDs MoS_2 and WS_2. Our fluorescence-based live−dead assay, reactive oxygen species assay, and mutagenic assay all strongly suggest that both 2D sheets and quasi-2D nanoparticulates of WS_2 and MoS_2 are biocompatible and nonmutagenic toward HEK293f human kidney cells and *S. typhimurium* TA100 bacteria, respectively. We found that the TMD materials did not trigger the generation of high levels of ROS that accompanies cell death. Even after prolonged exposure to concentrations as high as 100 μg/mL of TMDs, *S. typhimurium* bacteria did not significantly mutate. The results of our investigation pave the way for the use of 2D ME-WS_2, ME-MoS_2, and CVD MoS_2 in medical implantations, and highlights areas where additional investigations of biocompatibility will be important for adoption into implants and other biological systems.

ASSOCIATED CONTENT

Supporting Information

The Supporting Information is available free of charge on the ACS Publications website at DOI: 10.1021/acsbiomaterials.5b00467.

Figures S1−S6 showing SEM images of control materials, raw ROS fluorescent images, fluorescent intensity plots of ROS generated by cells in contact with flake/sheet forms of MoS_2, results from a live−dead assay examining particulate ME-MoS_2, and images of the raw mutagenic data (PDF)

AUTHOR INFORMATION

Corresponding Author

*E-mail: Junseok.Chae@asu.edu.

Notes

The authors declare no competing financial interest.

ACKNOWLEDGMENTS

We thank Dr. Julien Chen for HEK293f cell culture protocols. Q.H.W. and A.A.G. acknowledge support from Arizona State University startup funds. This work is supported by the NSF Graduate Research Fellowship under Grant DGE-1311230.

REFERENCES

(1) (a) Xu, M.; Liang, T.; Shi, M.; Chen, H. Graphene-like two-dimensional materials. *Chem. Rev.* **2013**, *113*, 3766−379810. (b) Neto, A. H. C.; Novoselov, K. Two-Dimensional Crystals: Beyond Graphene. *Mater. Express* **2011**, *1* (1), 10−17.

(2) (a) Mak, K. F.; Lee, C.; Hone, J.; Shan, J.; Heinz, T. F. Atomically thin MoS2: A new direct-gap semiconductor. *Phys. Rev. Lett.* **2010**, *105*, 2−5. (b) Song, X.; Hu, J.; Zeng, H. Two-dimensional semiconductors: recent progress and future perspectives. *J. Mater. Chem. C* **2013**, *1*, 2952.

(3) Wang, Q. H.; Kalantar-Zadeh, K.; Kis, A.; Coleman, J. N.; Strano, M. S. Electronics and optoelectronics of two-dimensional transition metal dichalcogenides. *Nat. Nanotechnol.* **2012**, *7*, 699−712.

(4) He, Z.; Sheng, Y.; Rong, Y.; Lee, G.-d.; Li, J.; Warner, J. H. Layer-dependent modulation of tungsten disulfide photoluminescence by lateral electric fields. *ACS Nano* **2015**, *9*, 2740−2748.

DOI: 10.1021/acsbiomaterials.5b00467
ACS Biomater. Sci. Eng. 2016, 2, 361−367

(5) Castellanos-Gomez, A.; Poot, M.; Steele, G. a.; Van Der Zant, H. S. J.; Agraït, N.; Rubio-Bollinger, G. Elastic properties of freely suspended MoS 2 nanosheets. *Adv. Mater.* **2012**, *24*, 772−775.
(6) (a) Tenne, R. Advances in the synthesis of inorganic nanotubes and fullerene- like nanoparticles. *Angew. Chem., Int. Ed.* **2003**, *42*, 5124−5132. (b) Tenne, R. Recent advances in the research of inorganic nanotubes and fullerene-like nanoparticles. *Frontiers of Physics* **2014**, *9*, 370−377. (c) Tenne, R.; Seifert, G. Recent Progress in the Study of Inorganic Nanotubes and Fullerene-Like Structures. *Annu. Rev. Mater. Res.* **2009**, *39*, 387−413.
(7) Tenne, R.; Redlich, M. Recent advances in the research of inorganic nanotubes and fullerene-like nanoparticles. *Chem. Soc. Rev.* **2010**, *39*, 1423−1434.
(8) Redlich, M.; Katz, A.; Rapoport, L.; Wagner, H. D.; Feldman, Y.; Tenne, R. Improved orthodontic stainless steel wires coated with inorganic fullerene-like nanoparticles of WS2 impregnated in electroless nickel-phosphorous film. *Dent. Mater.* **2008**, *24*, 1640−1646.
(9) Goldbart, O.; Sedova, A.; Yadgarov, L.; Rosentsveig, R.; Shumalinsky, D.; Lobik, L.; Wagner, H. D.; Tenne, R. Lubricating Medical Devices with Fullerene-Like Nanoparticles. *Tribol. Lett.* **2014**, *55*, 103−109.
(10) Lalwani, G.; Henslee, A. M.; Farshid, B.; Parmar, P.; Lin, L.; Qin, Y. X.; Kasper, F. K.; Mikos, A. G.; Sitharaman, B. Tungsten disulfide nanotubes reinforced biodegradable polymers for bone tissue engineering. *Acta Biomater.* **2013**, *9*, 8365−8373.
(11) Goldman, E. B.; Zak, A.; Tenne, R.; Kartvelishvily, E.; Levin-Zaidman, S.; Neumann, Y.; Stiubea-Cohen, R.; Palmon, A.; Hovav, A.-H.; Aframian, D. J. Biocompatibility of tungsten disulfide inorganic nanotubes and fullerene-like nanoparticles with salivary gland cells. *Tissue Eng., Part A* **2015**, *21*, 1013−1023.
(12) Wu, H.; Yang, R.; Song, B.; Han, Q.; Li, J.; Zhang, Y.; Fang, Y.; Tenne, R.; Wang, C. Biocompatible inorganic fullerene-like molybdenum disulfide nanoparticles produced by pulsed laser ablation in water. *ACS Nano* **2011**, *5*, 1276−1281.
(13) Teo, W. Z.; Chng, E. L. K.; Sofer, Z.; Pumera, M. Cytotoxicity of exfoliated transition-metal dichalcogenides (MoS 2, WS2, and WSe2) is lower than that of graphene and its analogues. *Chem. - Eur. J.* **2014**, *20*, 9627−9632.
(14) Liu, T.; Wang, C.; Gu, X.; Gong, H.; Cheng, L.; Shi, X.; Feng, L.; Sun, B.; Liu, Z. Drug delivery with PEGylated MoS2 nano-sheets for combined photothermal and chemotherapy of cancer. *Adv. Mater.* **2014**, *26*, 3433−3440.
(15) (a) Takenaka, S.; Karg, E.; Roth, C.; Schulz, H.; Ziesenis, A.; Heinzmann, U.; Schramel, P.; Heyder, J. Pulmonary and systemic distribution of inhaled ultrafine silver particles in rats. *Environ. Health Perspect.* **2001**, *109*, 547−551. (b) Ballestri, M.; Baraldi, A.; Gatti, A. M.; Furci, L.; Bagni, A.; Loria, P.; Rapanà, R. M.; Carulli, N.; Albertazzi, A. Liver and kidney foreign bodies granulomatosis in a patient with malocclusion, bruxism, and worn dental prostheses. *Gastroenterology* **2001**, *121*, 1234−1238.
(16) Osman, O.; Zanini, L. F.; Frénéa-Robin, M.; Dumas-Bouchiat, F.; Dempsey, N. M.; Reyne, G.; Buret, F.; Haddour, N. Monitoring the endocytosis of magnetic nanoparticles by cells using permanent microflux sources. *Biomed. Microdevices* **2012**, *14*, 947−954.
(17) Jiang, W.; Kim, B. Y. S.; Rutka, J. T.; Chan, W. C. W. Nanoparticle-mediated cellular response is size-dependent. *Nat. Nanotechnol.* **2008**, *3*, 145−150.
(18) (a) Song, J. G.; Park, J.; Lee, W.; Choi, T.; Jung, H.; Lee, C. W.; Hwang, S. H.; Myoung, J. M.; Jung, J. H.; Kim, S. H.; Lansalot-Matras, C.; Kim, H. Layer-controlled, wafer-scale, and conformal synthesis of tungsten disulfide nanosheets using atomic layer deposition. *ACS Nano* **2013**, *7*, 11333−11340. (b) Gutierrez, H. R.; Perea-Lopez, N.; Elias, A. L.; Berkdemir, A.; Wang, B.; Lv, R.; Lopez-Urias, F.; Crespi, V. H.; Terrones, H.; Terrones, M. Extraordinary room-temperature photoluminescence in triangular WS 2 monolayers. *Nano Lett.* **2013**, *13*, 3447−3454.
(19) Lee, C.; Yan, H.; Brus, L. E.; Heinz, T. F.; Hone, Ḱ. J.; Ryu, S. Anomalous Lattice Vibrations of Single- and Few-Layer MoS2. *ACS Nano* **2010**, *4*, 2695−2700.
(20) Liao, K. H.; Lin, Y. S.; MacOsko, C. W.; Haynes, C. L. Cytotoxicity of graphene oxide and graphene in human erythrocytes and skin fibroblasts. *ACS Appl. Mater. Interfaces* **2011**, *3*, 2607−2615.
(21) Bratosin, D.; Mitrofan, L.; Palii, C.; Estaquier, J.; Montreuil, J. Novel fluorescence assay using calcein-AM for the determination of human erythrocyte viability and aging. *Cytometry, Part A* **2005**, *66*, 78−84.
(22) Skala, M. C.; Squirrell, J. M.; Vrotsos, K. M.; Eickhoff, J. C.; Gendron-Fitzpatrick, A.; Eliceiri, K. W.; Ramanujam, N. Multiphoton microscopy of endogenous fluorescence differentiates normal, precancerous, and cancerous squamous epithelial tissues. *Cancer Res.* **2005**, *65*, 1180−1186.
(23) Graham, F. L.; Smiley, J.; Russell, W. C.; Nairn, R. Characteristics of a Human Cell Line Transformed by DNA from Human Adenovirus Type 5. *J. Gen. Virol.* **1977**, *36*, 59−72.
(24) Chen, G. Y.; Pang, D. W. P.; Hwang, S. M.; Tuan, H. Y.; Hu, Y. C. A graphene-based platform for induced pluripotent stem cells culture and differentiation. *Biomaterials* **2012**, *33*, 418−427.
(25) Łopacińska, J. M.; Emnéus, J.; Dufva, M. Poly-(Dimethylsiloxane) (PDMS) Affects Gene Expression in PC12 Cells Differentiating into Neuronal-Like Cells. *PLoS One* **2013**, *8*, e53107.
(26) de Lima, R.; Seabra, A. B.; Durán, N. Silver nanoparticles: A brief review of cytotoxicity and genotoxicity of chemically and biogenically synthesized nanoparticles. *J. Appl. Toxicol.* **2012**, *32*, 867−879.
(27) Anderson, J. M.; Rodriguez, A.; Chang, D. T. Foreign Body Reaction to Biomaterials. *Semin. Immunol.* **2008**, *20*, 86−100.
(28) Ayala, V.; Herrera, A. P.; Latorre-Esteves, M.; Torres-Lugo, M.; Rinaldi, C. Effect of surface charge on the colloidal stability and in vitro uptake of carboxymethyl dextran-coated iron oxide nanoparticles. *J. Nanopart. Res.* **2013**, *15*, 1874.
(29) Circu, M. L.; Aw, T. Y. Reactive oxygen species, cellular redox systems, and apoptosis. *Free Radical Biol. Med.* **2010**, *48*, 749−762.
(30) Elahi, M. M.; Kong, Y. X.; Matata, B. M. Oxidative stress as a mediator of cardiovascular disease. *Oxid. Med. Cell. Longevity* **2009**, *2*, 259−269.
(31) Alarifi, S.; Ali, D.; Verma, A.; Alakhtani, S.; Ali, B. A. Cytotoxicity and genotoxicity of copper oxide nanoparticles in human skin keratinocytes cells. *Int. J. Toxicol.* **2013**, *32*, 296−307.
(32) Splendiani, A.; Sun, L.; Zhang, Y.; Li, T.; Kim, J.; Chim, C.-y.; Galli, G.; Wang, F. Emerging Photoluminescence in Monolayer MoS2. *Nano Lett.* **2010**, *10*, 1271−1275.
(33) Li, Y.; Chen, D. H.; Yan, J.; Chen, Y.; Mittelstaedt, R. A.; Zhang, Y.; Biris, A. S.; Heflich, R. H.; Chen, T. Genetic Toxicology and Environmental Mutagenesis Genotoxicity of silver nanoparticles evaluated using the Ames test and in vitro micronucleus assay. *Mutat. Res., Genet. Toxicol. Environ. Mutagen.* **2012**, *745*, 4−10.
(34) Woodruff, R. S.; Li, Y.; Yan, J.; Bishop, M.; Jones, M. Y.; Watanabe, F.; Biris, A. S.; Rice, P.; Zhou, T.; Chen, T. Genotoxicity evaluation of titanium dioxide nanoparticles using the Ames test and Comet assay. *J. Appl. Toxicol.* **2012**, *32*, 934−943.
(35) Mao, W. P.; Ye, J. L.; Guan, Z. B.; Zhao, J. M.; Zhang, C.; Zhang, N. N.; Jiang, P.; Tian, T. Cadmium induces apoptosis in human embryonic kidney (HEK) 293 cells by caspase-dependent and -independent pathways acting on mitochondria. *Toxicol. In Vitro* **2007**, *21*, 343−354.
(36) Kou, Z.; Wang, X.; Yuan, R.; Chen, H.; Zhi, Q.; Gao, L.; Wang, B.; Guo, Z.; Xue, X.; Cao, W.; Guo, L. A promising gene delivery system developed from PEGylated MoS2 nanosheets for gene therapy. *Nanoscale Res. Lett.* **2014**, *9*, 587.

DOI: 10.1021/acsbiomaterials.5b00467
ACS Biomater. Sci. Eng. 2016, 2, 361−367